



Photoinduced Mn doping in cesium lead halide perovskite nanocrystals

Journal:	<i>Nanoscale</i>
Manuscript ID	NR-ART-12-2018-010439.R1
Article Type:	Paper
Date Submitted by the Author:	04-Mar-2019
Complete List of Authors:	Qiao, Tian; Texas A&M University College Station, Department of Chemistry Parobek, David; Texas A&M University College Station, Department of Chemistry Dong, Yitong; Texas A and M University College Station, Department of Chemistry Ha, Eunsang; Texas A and M University College Station, Department of Chemistry Son, Dong Hee; Texas A&M University College Station, Department of Chemistry

Photoinduced Mn doping in cesium lead halide perovskite nanocrystals

Tian Qiao[†], David Parobek[†], Yitong Dong[†], Eunsang Ha[†] and Dong Hee Son^{*,†,‡}

[†]Department of Chemistry, Texas A&M University, College Station, Texas 77843, United States

[‡]Center for Nanomedicine, Institute for Basic Science (IBS), Seoul 03722, Republic of Korea

Abstract

We report the photoinduced post-synthesis method of Mn doping in colloidal perovskite nanocrystals, which can produce Mn-doped CsPbX₃ (X=Cl, Br) nanocrystals with preserved size and anisotropic morphology. Photoinduced Mn doping occurs through cation exchange driven by the facile photoinduced halide exchange in dihalomethane (CH₂X₂, X=Cl, Br) solvent taking advantage of *in-situ* photogeneration of halide ion from the solvent molecules. In the presence of a small amount of Mn acetate dissolved in solvent at sub-micromolar concentration, photoexcitation of the nanocrystals above the bandgap initiates the simultaneous anion and cation exchange. Under the condition of self-anion exchange, the resulting product is only the cation (Mn) doping in the nanocrystal host without changing halide composition, where the extent of doping can be controlled by excitation light intensity. The mild nature of the photoinduced doping also preserves the anisotropic morphology of the nanocrystals. The photoinduced Mn-doping method could be further expanded to other cations providing a versatile means of creating various cation-doped perovskite nanocrystals that are difficult to produce by other means.

Introduction

Semiconducting lead halide nanocrystals have attracted much interest due to their excellent optical and optoelectronic properties including large absorption cross-section¹ and high photoluminescence quantum yield.^{2,3} Like in other semiconductor nanocrystals,⁴⁻⁶ various optical and electronic properties of lead halide perovskite nanocrystals are controllable by tuning the halide composition or doping. Variation of anion composition via post-synthesis anion exchange⁷⁻⁹ has been extensively utilized to chemically tune the bandgap of these materials throughout the visible spectral range. The highly labile nature of halide ions within the lattice of lead halide nanocrystals enabled the facile anion exchange even at room temperature, making the post-synthesis anion exchange a highly versatile method of tuning anion composition. Variation of the cation composition has also been pursued to produce lead-free perovskite nanocrystals¹⁰⁻¹² or to introduce new photophysical properties¹³⁻²⁷ originating from the dopant. In particular, substitutional doping of Pb²⁺ with transition metal¹³⁻²¹ or rare-earth metal²⁷ ions such as Mn²⁺ and Yb³⁺ have been studied extensively for the strong sensitized luminescence. However, post-synthesis cation exchange is significantly more difficult than anion exchange,^{28,29} therefore less utilized as the method of post-synthesis cation doping.

Recently, post-synthesis doping of Mn²⁺ ions in CsPbX₃ nanocrystals *via* simultaneous anion and cation exchange was demonstrated in several studies.²⁹⁻³¹ In these studies, doping of Mn²⁺ was considered to result from the cation exchange driven by the halide exchange. For this reason, conditions enabling the halide exchange were necessary to induce doping *via* cation exchange. While the halide exchange has been mostly achieved by adding a reactive halide source, we have recently shown that dihalomethane (CH₂X₂) used as the solvent can generate halide ion *in-situ* enabling facile photoinduced anion exchange in perovskite without using a separate halide source.⁸ The *in-situ* photoinduced generation of halide is possible because of the interfacial electron transfer from the photoexcited perovskite nanocrystals to CH₂X₂ molecules near the surface, resulting in the reductive dissociation of C-X bond producing X⁻. The photoinduced halide exchange benefits from the easy control of the extent of reaction *via* photon dose in addition to not requiring a separate halide other than solvent itself. It is also capable of spatially patterning the chemical transformation since photoexcitation is necessary to initiate the exchange process. Here, we show that photoinduced doping of Mn²⁺ in CsPbX₃ (X=Cl, Br) nanocrystals can be achieved by taking

advantage of photoinduced halide exchange in CH_2X_2 solvent. CH_2X_2 is sufficiently nonpolar to keep highly ionic CsPbX_3 nanocrystals intact during the reaction and is also able to dissolve a sufficient amount of the precursor of Mn^{2+} , such as Mn acetate, necessary for the photoinduced cation exchange. In this work, we demonstrate the unique benefits of photoinduced cation exchange that can produce various Mn-doped CsPbX_3 ($\text{X}=\text{Cl}, \text{Br}$) nanocrystals exhibiting sensitized Mn luminescence that also preserves the anisotropic morphology.

Experimental

Synthesis of CsPbCl_3 nanocubes: CsPbCl_3 nanocubes were synthesized using a previously reported method² with slight modifications. The Cs precursor (Cs-oleate) solution was prepared by mixing Cs_2CO_3 (0.25 g), oleic acid (OA, 0.8 g) and 1-octadecene (ODE, 7g) and heating to 150 °C until all Cs_2CO_3 is dissolved. The Pb/Cl precursor solution was prepared by heating the mixture of PbCl_2 (90 mg), oleylamine (OAm, 1mL) and OA (1 mL) at 200 °C. The reaction was initiated by injecting 0.4 mL of Cs-oleate solution to the Pb/Cl precursor solution maintained at 200 °C. After 1 min of reaction, the reaction was quenched by cooling in an ice water bath. The produced CsPbCl_3 nanocubes were precipitated with acetone and collected after centrifugation.

Synthesis of CsPbCl_3 nanorods: CsPbCl_3 nanorods (~2 nm in diameter) were synthesized at room temperature by adding acetone to the mixture of Cs-oleate solution and Pb/Cl precursor solution. The Pb/Cl precursor solution was prepared by heating the mixture of PbCl_2 (60 mg), CuCl_2 (200 mg), OAm (~2 mL) and OA (~2 mL) at 200 °C, which was subsequently cooled to room temperature. In the mixture of both precursor solutions, ~10 mL of acetone was added to initialize the growth of CsPbCl_3 nanorods. The produced nanorods were precipitated and collected by centrifugation.

Synthesis of CsPbBr_3 quantum dots: ~4 nm CsPbBr_3 quantum dots were synthesized using the recently reported method.³² PbBr_2 (80 mg) and ZnBr_2 (250 mg) were mixed with dried OAm (~2mL) and OA (~2 mL) followed by an injection of 0.4 mL of Cs-oleate solution at 80 °C. The reaction was maintained for 2 mins at 80 °C and subsequently quenched in an ice bath. The nanocrystals were recovered by centrifuging the reactant mixture after adding acetone.

Photoinduced Mn doping: CH_2X_2 (X=Cl, Br) solution of Mn acetate tetrahydrate ($(\text{CH}_3\text{COO})_2\text{Mn}\cdot 4\text{H}_2\text{O}$) was prepared by first sonicating the salt in the solvent for 30 mins. The solution was filtered with a polytetrafluoroethylene (PTFE) filter to remove the undissolved Mn salt to obtain the saturated solution of Mn acetate in CH_2X_2 . The concentration of Mn determined from elemental analysis was $0.4 \mu\text{M}$. Perovskite nanocrystals were dispersed in these solutions at varying concentrations of Mn^{2+} and nanocrystals. The photoexcitation that initiates Mn doping was performed using UV light-emitting diode (LED) with the emission centered at 365 nm with fwhm of 10 nm. For CsPbCl_3 nanorods, the LED was able to excite the red side of exciton emission.

Optical and structural characterization of the nanocrystals: Absorption and photoluminescence (PL) spectra of the samples were obtained using fiberoptic-coupled CCD spectrometers (Ocean Optics, USB4000 and QE65). PL spectra were obtained at the excitation wavelength of 350 nm (300 nm for CsPbCl_3 nanorods). For Mn luminescence lifetime measurement, a pulsed N_2 laser (NL100 SRS, 337 nm) was used as the excitation source. The signal from the photomultiplier tube (R928, Hamamatsu) coupled to an amplifier was recorded with a digital oscilloscope (WaveAce 234, Lecroy). Photoluminescence excitation (PLE) spectra were taken with PTI QuantaMaster fluorometer by measuring the intensity of Mn luminescence at 600 nm, using a Xe lamp as a tunable excitation source. TEM images of perovskite nanocrystals were collected on FEI Tecnai G2 F20 ST FE-TEM microscope. Mn-doping concentration was determined using inductively coupled plasma mass spectrometry (ICP-MS, NexIon 300D). Methyl acetate was used as an anti-solvent to precipitate and purify the nanocrystals out of their concentrated solutions. The precipitation and purification steps were repeated at least three times to thoroughly remove unreacted Mn. Electron paramagnetic resonance (EPR) spectra were obtained on Bruker E1 Exsys with a super CW EPR bridge. EPR signals were obtained at room temperature with 9.37 MHz microwave frequency and 20 mW microwave power.

Results and discussion

Figure 1a shows the photoluminescence (PL) spectra of CsPbCl_3 nanocrystals dispersed in CH_2Cl_2 in the presence of dissolved Mn (II) acetate ($0.4 \mu\text{M}$) under photoexcitation by a UV LED (center $\lambda=365$ nm, fwhm=10nm) at the intensity of 14 mW/cm^2 with varying photoexcitation

times. Within 2 mins of photoexcitation, Mn luminescence centered at 628 nm was observed indicating the presence of doped Mn^{2+} in the nanocrystal that allows the sensitization of Mn $d-d$ transition by exciton. With increasing photoexcitation time, Mn luminescence intensity continued to increase over several tens of minutes. In the absence of photoexcitation, no detectable Mn luminescence was observed indicating that the photoexcitation of the nanocrystal is the necessary process for Mn doping under our experimental condition. When CH_2Cl_2 is replaced with non-halogenated solvent such as hexane, no Mn luminescence was observed indicating that Mn doping is driven by halide exchange from *in-situ* photogenerated halide from CH_2Cl_2 . Figure 1b shows the time-dependent intensity of Mn luminescence intensity measured at several different photoexcitation times. The average lifetime of Mn luminescence is 0.3 ms, which is shorter than typical Mn luminescence lifetime in hot-injection synthesized nanocrystals.^{13, 18} We believe this is due to the relatively high local concentration of doped Mn^{2+} ions, resulting in antiferromagnetic coupling between Mn^{2+} ions that reduces Mn luminescence lifetime^{18, 33-35} as will be discussed further later. Figure 1c shows photoluminescence excitation (PLE) spectrum and the absorption spectrum, which are nearly identical to each other. This clearly indicates the presence of Mn^{2+} in the perovskite nanocrystals enabling the energy transfer from exciton to Mn^{2+} ions that gives rise to the observed Mn luminescence. Successful substitution of B-site Pb^{2+} with Mn^{2+} is further corroborated by X-band electron paramagnetic resonance (EPR) spectrum shown in Figure 1d, where the hyperfine splitting (86 Gauss) is identical to that of Mn-doped CsPbCl_3 nanocrystals prepared by hot-injection synthesis.¹³ TEM images and absorption spectra of CsPbCl_3 nanocrystals before and after the photoinduced Mn doping are shown in Figure 2. The size and morphology of the nanocrystals are preserved during the photoinduced Mn doping. The intensity of the absorption spectrum increased slightly after the photoinduced doping. Such increase in the absorption intensity was previously observed during the photoinduced halide exchange in CsPbCl_3 nanocrystals,⁸ which was considered to result from the removal of the existing Cl vacancy during the halide exchange process. The above results clearly indicate that doping of Mn^{2+} in CsPbCl_3 nanocrystals can be achieved by the cation exchange driven by the photoinduced halide exchange.

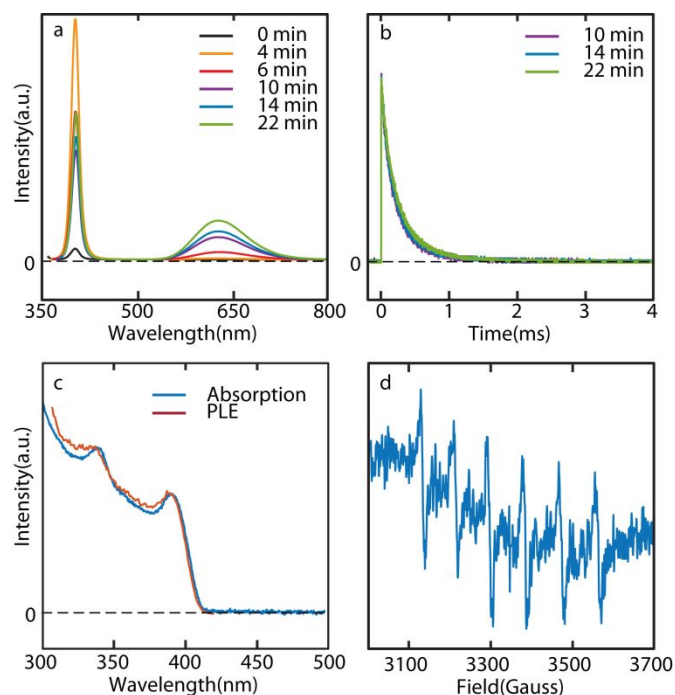


Figure 1. (a,b) PL spectra (a) and time-dependent Mn luminescence intensity (b) of CsPbCl₃ nanocrystals undergoing the photoinduced Mn doping by a UV LED at the intensity of 14 mW/cm² and varying photoexcitation times. (c) Absorption spectrum (blue) and photoluminescence excitation (PLE) spectrum (red) measured at 600 nm. d, Electron paramagnetic resonance (EPR) spectrum of Mn-doped CsPbCl₃ prepared *via* photoinduced doping.

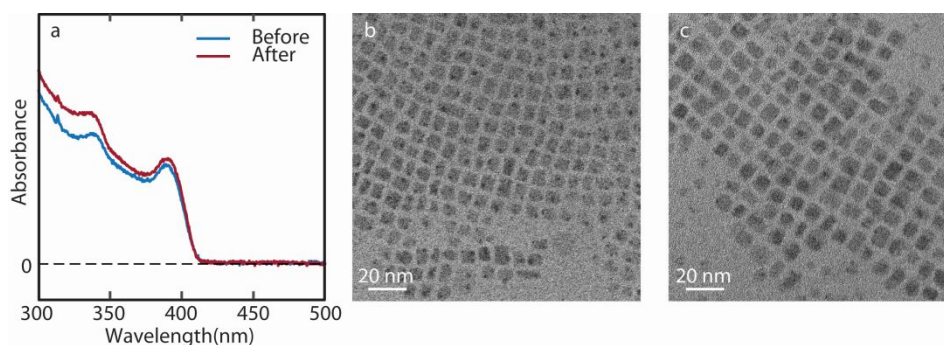


Figure 2. (a) Absorption spectra of CsPbCl₃ nanocrystals before (blue) and after (red) photoinduced Mn doping. (b,c) TEM image of CsPbCl₃ nanocrystals before (b) and after (c) the photoinduced Mn doping.

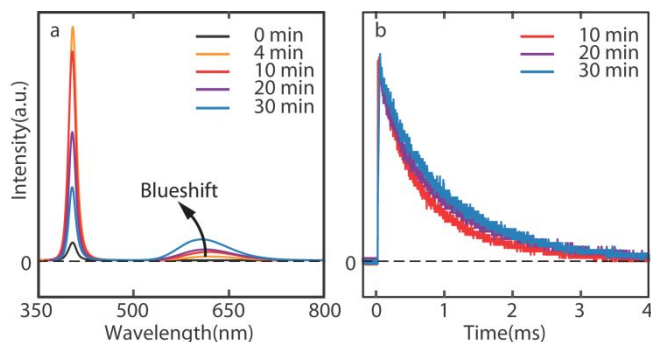


Figure 3. PL spectra (a) and time-dependent Mn luminescence intensity (b) of CsPbCl₃ nanocrystals undergoing the photoinduced Mn doping by 365 nm light at the intensity of 100 mW/cm² and varying photoexcitation times.

Since Mn doping requires the photoinduced halide exchange, the intensity of light that directly controls the rate of halide exchange should dictate the extent and the rate of Mn doping. To examine the effect of varying excitation light intensity on photoinduced Mn doping, an additional experiment was performed at the higher excitation intensity. Figure 3a shows the PL spectra of CsPbCl₃ nanocrystals undergoing the photoinduced doping of Mn at the excitation intensity of 100 mW/cm². Figure 3b shows the time-dependent intensity of Mn luminescence measured at several different photoexcitation times. Two major differences are observed in the PL spectra and time-dependent Mn luminescence intensity between the lower (Figure 1, 14 mW/cm²) and the higher (Figure 3, 100 mW/cm²) excitation intensities when the comparable reaction times are used. In contrast to Figure 1a that shows a negligible spectral shift of Mn luminescence centered at 628 nm, Figure 3a shows a continuous blueshift of Mn PL with increasing photoexcitation time from 625 to 610 nm. Furthermore, the average lifetime of Mn luminescence in Figure 3b is much longer (~1 ms) and exhibits gradually increasing lifetime with continued photoinduced Mn doping. The blueshift of Mn PL energy and the increase of Mn PL lifetime in Figure 3a and 3b are indicative of increasing Mn-Mn distance and the decreasing effect of Mn-Mn exchange coupling on Mn luminescence. The longer Mn luminescence lifetime under the higher photoexcitation can also be interpreted as the larger Mn-Mn distance and weaker effect of Mn-Mn exchange coupling on Mn luminescence. At first glance, the larger Mn-Mn distance may appear contradictory to the higher excitation intensity that should increase the photoinduced doping rate. However, it can be

explained by different local Mn doping concentration and spatial extent of Mn doping within the nanocrystals affected by the rate of photoinduced halide exchange process that drives Mn doping.

The apparently stronger effect of Mn-Mn exchange coupling observed in the nanocrystals at the weaker photoexcitation intensity (14 mW/cm^2) could be explained by the higher local density of Mn^{2+} ions that are largely localized closer to the surface of the nanocrystals. Near absence of the shift of Mn PL in Figure 1 indicates that local doping density of Mn^{2+} ions is not changing significantly under the given excitation condition. According to the earlier study, the Mn luminescence lifetime in CsPbCl_3 nanocrystal host decreases to 0.3 ms above the doping concentration of 14%.¹⁸ Mn doping concentration of CsPbCl_3 nanocrystals in this study determined from the inductive coupled plasma mass spectrometry (ICP-MS) is $\sim 2\%$, which suggests the highly non-uniform doping within the nanocrystal. Since Mn doping occurs *via* cation exchange facilitated by the photoinduced anion exchange at room temperature, spatially more heterogeneous doping compared to hot-injection synthesis may not be unexpected. On the other hand, blue shift of Mn PL was observed under much longer photoexcitation ($>1 \text{ hr}$) indicating a slow and gradual movement of Mn^{2+} ions to from near the surface to further into the interior of the nanocrystals. In contrast, more rapid halide and cation exchange at the higher photoexcitation intensity (100 mW/cm^2) may result in Mn doping over the large space within the nanocrystal for the same reaction time. The blueshift of Mn PL and elongation of its lifetime with continued photoexcitation can be accounted for by the increasing Mn-Mn distance from the expanded spatial extent of doping within the nanocrystals despite the increasing overall level of doping. The above observation suggests the possible control of the spatial distribution of Mn^{2+} ions by varying both the excitation light intensity and the concentration of Mn^{2+} in the solvent medium, although this study will not address this in depth. In the case of Mn-doped II-VI quantum dots, the ability to control the radial doping location within the nanocrystal during the synthesis enabled the structural control of the exchange coupling between exciton and dopant that determines the energy transfer rate.³³ While such control would be difficult in hot injection synthesis of Mn-doped perovskite nanocrystals, the post-synthesis photoinduced Mn doping can enable some control over the doping structure.

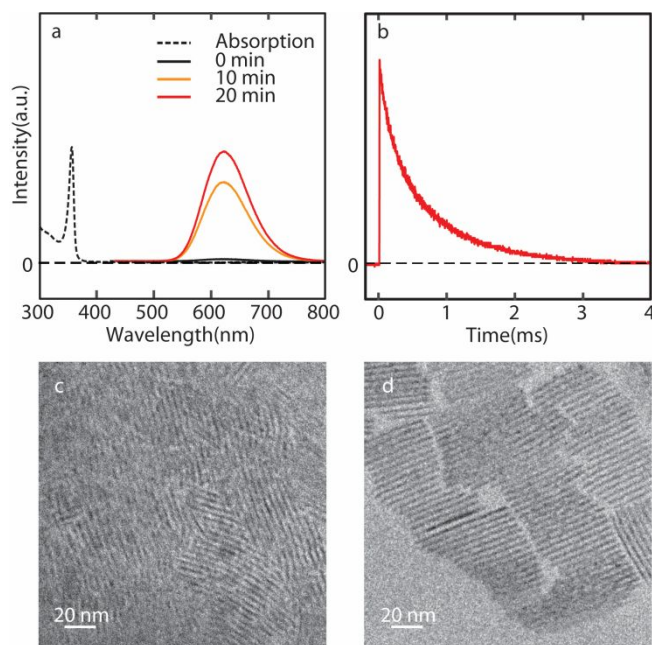


Figure 4. (a) Absorption (dashed) and PL spectra (solid) of CsPbCl₃ nanorods undergoing the photoinduced Mn doping by a UV LED at the intensity of 100 mW/cm² and varying photoexcitation times. (b) Time-dependent Mn luminescence intensity of CsPbCl₃ nanorods after 20 mins of photoexcitation. (c,d) TEM image of CsPbCl₃ nanorods before (c) and after (d) the photoinduced Mn doping.

One distinct advantage of post-synthesis photoinduced Mn doping at room temperature compared to hot-injection synthesis is the possible preservation of the morphology of the anisotropic nanocrystals. Various anisotropic optical and transport properties can be harvested in the nanocrystals of anisotropic morphology by controlling their orientation.³⁶⁻³⁸ To confirm the capability of photoinduced Mn doping to preserve the anisotropic morphology of the host nanocrystals, the reaction was performed on CsPbCl₃ nanorods that exhibit excitonic absorption peak near 350 nm. The thickness of the nanorods is ~2 nm, which exhibits strongly blueshifted exciton peak ($\lambda=356$ nm) with respect to the larger nanocrystals due to the quantum confinement. Figure 4a shows PL spectra of CsPbCl₃ nanorods undergoing the photoinduced Mn doping by a UV LED at different photoexcitation times together with the absorption spectrum. Because of the relatively broad spectrum of the UV LED, it was still able to excite CsPbCl₃ nanorods on the red side of the exciton peak. The time-dependent Mn PL intensity after 20 mins of photoexcitation is

shown in Figure 4b. The average lifetime of Mn PL is 0.8 ms. TEM images of CsPbCl₃ nanorods before and after the photoinduced Mn doping are shown in Figure 4c and d respectively, which show the preservation of the anisotropic morphology of the host nanocrystals.

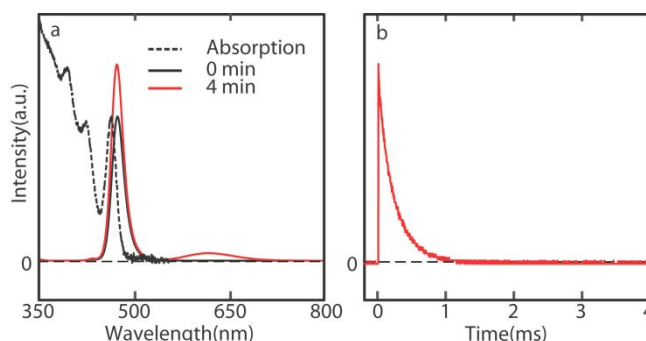


Figure 5. (a) Absorption (dashed) and PL spectra (solid) of CsPbBr₃ quantum dots undergoing the photoinduced Mn doping by a UV LED at the intensity of 14 mW/cm². (b) Time-dependent Mn luminescence intensity of CsPbBr₃ quantum dots after 4 mins of reaction.

Doping of Mn via photoinduced cation exchange facilitated by the simultaneous halide exchange should in principle be applied to CsPbBr₃ nanocrystals. In hot-injection synthesis of Mn-doped perovskite nanocrystals, doping Mn²⁺ ions in CsPbBr₃ host has been significantly more challenging than in CsPbCl₃ host. One strategy that has been recently developed to produce Mn-doped CsPbBr₃ is utilizing Mn-doped 2-dimensional monolayer structure of L₂PbBr₄ (L: ligand)¹⁹ that subsequently transforms into Mn-doped CsPbBr₃ nanocrystals. Here, we examined whether the photoinduced Mn doping can be achieved in CsPbBr₃ nanocrystals by using CH₂Br₂ as the solvent in the presence of dissolved Mn acetate. Figure 5a shows the PL spectra of CsPbBr₃ nanocrystals undergoing the photoinduced Mn doping by a UV LED at the intensity of 14 mW/cm² together with the absorption spectrum. The size of CsPbBr₃ nanocrystals are ~4 nm and exhibits exciton absorption peak at 465 nm due to the quantum confinement, which is sufficient to allow the energy transfer from exciton to Mn giving rise to the sensitized Mn luminescence. The time-dependent Mn luminescence intensity after 4 mins of photoexcitation is shown in Figure 5b. The lifetime of Mn PL is ~0.2 ms, which is similar to what was reported for Mn-doped CsPbBr₃

nanocrystals synthesized directly via hot-injection method.¹⁹ These results clearly show that photoinduced Mn doping can also be achieved in CsPbBr₃ nanocrystal host. Under our current non-optimized reaction condition, prolonged photoexcitation resulted in the redshift of the exciton emission, suggesting the growth of the particle size. Nevertheless, we anticipate the preservation of the morphology and size could be achieved with further optimization of the reaction condition. The result above indicates that photoinduced doping is a very useful post-synthesis cation doping method for obtaining CsPbBr₃ nanocrystals with sensitized dopant emission, since the majority of the earlier post-synthesis approach were unsuccessful.^{29, 30}

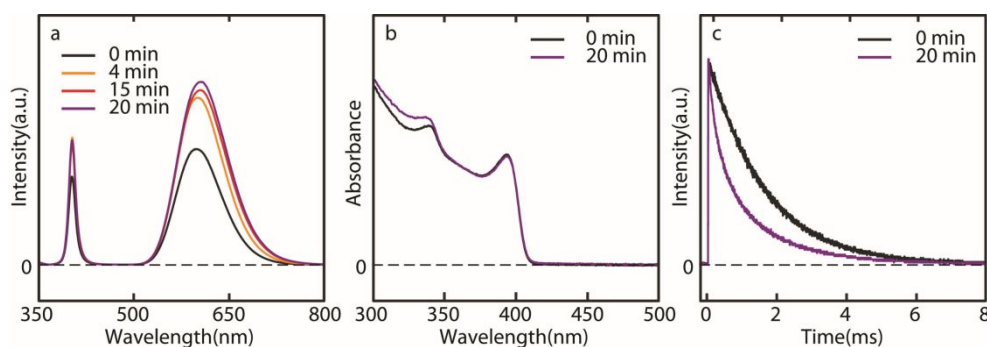


Figure 6. (a,b) PL spectra (a), absorption spectra (b) and time-dependent Mn luminescence intensity (c) of Mn-doped CsPbCl₃ nanocrystals undergoing the photoinduced Mn doping by a UV LED at the intensity of 100 mW/cm² and varying photoexcitation times.

Photoinduced doping of Mn can also be applied to the nanocrystals already doped with Mn²⁺ ions to further modify the doping structure in the nanocrystals. Figure 6a shows the PL spectra of hot-injection synthesized Mn-doped CsPbCl₃ nanocrystals undergoing the additional photoinduced Mn doping by a UV LED at the intensity of 100 mW/cm². Figure 6b shows the absorption spectra of Mn-doped CsPbCl₃ nanocrystals before and after the photoinduced Mn doping, which shows little change of the absorption spectrum. Figure 6c compares the time-dependent Mn luminescence intensities before and after the photoinduced Mn doping. The increase of the Mn luminescence intensity and the decrease of Mn PL lifetime indicate that the doping concentration in the pre-doped nanocrystals can be further increased *via* photoinduced Mn doping.

This demonstrates the versatility of photoinduced Mn doping to access the wider range of doping concentration by using pre-doped nanocrystals as the starting material.

Conclusion

In conclusion, we demonstrated the post-synthesis photoinduced Mn doping in perovskite nanocrystals that can produce Mn-doped CsPbX_3 ($X=\text{Cl}, \text{Br}$) nanocrystals of varying morphologies exhibiting sensitized Mn luminescence. The photoinduced Mn doping takes advantage of the recently developed photoinduced anion exchange, where CH_2X_2 ($X=\text{Cl}, \text{Br}$) used as the solvent generates halide in-situ via photoinduced reductive dissociation on the surface of the nanocrystals. In the presence of small amount of dissolved Mn acetate in CH_2X_2 , photoexcitation resulted in the cation exchange driven by the halide exchange resulting in the formation of Mn-doped CsPbX_3 nanocrystals. Since the reaction requires the photoexcitation, the extent of reaction can be controlled by varying the excitation light intensity. Furthermore, the anisotropic morphology of the initial nanocrystals is preserved after the photoinduced doping, which is convenient for producing anisotropic doped nanocrystals that are otherwise difficult to produce. The new photoinduced doping method demonstrated here could be utilized for doping of other cations with appropriate choice of metal precursors, providing a versatile route to create various cation-doped perovskite nanocrystals.

Conflicts of interest

There are no conflicts to declare.

Acknowledgments

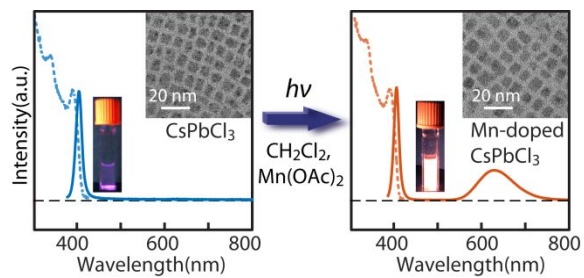
This work was supported by National Science Foundation CHE-1836538 (T.Q.), GRFP DGE-1252521 (D.P.) and Welch Foundation A-1639 (Y.D.). Support from IBS-R026-D1 (D.H.S) is also appreciated.

References

1. J. De Roo, M. Ibáñez, P. Geiregat, G. Nedelcu, W. Walravens, J. Maes, J. C. Martins, I. Van Driessche, M. V. Kovalenko and Z. Hens, *ACS Nano*, 2016, **10**, 2071-2081.
2. L. Protesescu, S. Yakunin, M. I. Bodnarchuk, F. Krieg, R. Caputo, C. H. Hendon, R. X. Yang, A. Walsh and M. V. Kovalenko, *Nano Lett.*, 2015, **15**, 3692-3696.
3. B. A. Koscher, J. K. Swabeck, N. D. Bronstein and A. P. Alivisatos, *J. Am. Chem. Soc.*, 2017, **139**, 6566-6569.
4. D. J. Norris, A. L. Efros and S. C. Erwin, *Science*, 2008, **319**, 1776-1779.
5. R. Beaulac, P. I. Archer, S. T. Ochsenein and D. R. Gamelin, *Adv. Funct. Mater.*, 2008, **18**, 3873-3891.
6. K. E. Knowles, K. H. Hartstein, T. B. Kilburn, A. Marchioro, H. D. Nelson, P. J. Whitham and D. R. Gamelin, *Chem. Rev.*, 2016, **116**, 10820-10851.
7. Q. A. Akkerman, V. D'Innocenzo, S. Accornero, A. Scarpellini, A. Petrozza, M. Prato and L. Manna, *J. Am. Chem. Soc.*, 2015, **137**, 10276-10281.
8. D. Parobek, Y. Dong, T. Qiao, D. Rossi and D. H. Son, *J. Am. Chem. Soc.*, 2017, **139**, 4358-4361.
9. D. Zhang, Y. Yang, Y. Bekenstein, Y. Yu, N. A. Gibson, A. B. Wong, S. W. Eaton, N. Kornienko, Q. Kong, M. Lai, A. P. Alivisatos, S. R. Leone and P. Yang, *J. Am. Chem. Soc.*, 2016, **138**, 7236-7239.
10. J. Zhu, X. Yang, Y. Zhu, Y. Wang, J. Cai, J. Shen, L. Sun and C. Li, *J. Phys. Chem. Lett.*, 2017, **8**, 4167-4171.
11. T. C. Jellicoe, J. M. Richter, H. F. J. Glass, M. Tabachnyk, R. Brady, S. E. Dutton, A. Rao, R. H. Friend, D. Credgington, N. C. Greenham and M. L. Böhm, *J. Am. Chem. Soc.*, 2016, **138**, 2941-2944.
12. A. B. Wong, Y. Bekenstein, J. Kang, C. S. Kley, D. Kim, N. A. Gibson, D. Zhang, Y. Yu, S. R. Leone, L.-W. Wang, A. P. Alivisatos and P. Yang, *Nano Lett.*, 2018, **18**, 2060-2066.
13. D. Parobek, B. J. Roman, Y. Dong, H. Jin, E. Lee, M. Sheldon and D. H. Son, *Nano Lett.*, 2016, **16**, 7376-7380.
14. W. Liu, Q. Lin, H. Li, K. Wu, I. Robel, J. M. Pietryga and V. I. Klimov, *J. Am. Chem. Soc.*, 2016, **138**, 14954-14961.
15. K. Xu, C. C. Lin, X. Xie and A. Meijerink, *Chem. Mater.*, 2017, **29**, 4265-4272.
16. S. Das Adhikari, S. K. Dutta, A. Dutta, A. K. Guria and N. Pradhan, *Angew. Chem.*, 2017, **129**, 8872-8876.
17. W. J. Mir, M. Jagadeeswararao, S. Das and A. Nag, *ACS Energy Lett.*, 2017, **2**, 537-543.
18. X. Yuan, S. Ji, M. C. De Siena, L. Fei, Z. Zhao, Y. Wang, H. Li, J. Zhao and D. R. Gamelin, *Chem. Mater.*, 2017, **29**, 8003-8011.
19. D. Parobek, Y. Dong, T. Qiao and D. H. Son, *Chem. Mater.*, 2018, **30**, 2939-2944.
20. B. J. Roman, J. Otto, C. Galik, R. Downing and M. Sheldon, *Nano Lett.*, 2017, **17**, 5561-5566.
21. Z. J. Yong, S. Q. Guo, J. P. Ma, J. Y. Zhang, Z. Y. Li, Y. M. Chen, B. B. Zhang, Y. Zhou, J. Shu, J. L. Gu, L. R. Zheng, O. M. Bakr and H. T. Sun, *J. Am. Chem. Soc.*, 2018, **140**, 9942-9951.
22. D. Rossi, D. Parobek, Y. Dong and D. H. Son, *J. Phys. Chem. C*, 2017, **121**, 17143-17149.
23. A. K. Guria, S. K. Dutta, S. D. Adhikari and N. Pradhan, *ACS Energy Lett.*, 2017, **2**, 1014-1021.
24. Y. Zhou, J. Chen, O. M. Bakr and H. T. Sun, *Chem. Mater.*, 2018, **30**, 6589-6613.

25. Z. Zhang, L. Ren, H. Yan, S. Guo, S. Wang, M. Wang and K. Jin, *J. Phys. Chem. C*, 2017, **121**, 17436-17441.
26. M. Liu, G. Zhong, Y. Yin, J. Miao, K. Li, C. Wang, X. Xu, C. Shen and H. Meng, *Adv. Sci.*, 2017, **4**, 1700335.
27. T. J. Milstein, D. M. Kroupa and D. R. Gamelin, *Nano Lett.*, 2018, **18**, 3792-3799.
28. W. van der Stam, J. J. Geuchies, T. Altantzis, K. H. W. van den Bos, J. D. Meeldijk, S. Van Aert, S. Bals, D. Vanmaekelbergh and C. de Mello Donega, *J. Am. Chem. Soc.*, 2017, **139**, 4087-4097.
29. G. Huang, C. Wang, S. Xu, S. Zong, J. Lu, Z. Wang, C. Lu and Y. Cui, *Adv. Mater.*, 2017, **29**, 1700095.
30. D. Chen, S. Zhou, G. Fang, X. Chen and J. Zhong, *ACS Appl. Mater. Interfaces*, 2018, **10**, 39872-39878.
31. W. J. Mir, Y. Mahor, A. Lohar, M. Jagadeeswararao, S. Das, S. Mahamuni and A. Nag, *Chem. Mater.*, 2018, **30**, 8170-8178.
32. Y. Dong, T. Qiao, D. Kim, D. Parobek, D. Rossi and D. H. Son, *Nano Lett.*, 2018, **18**, 3716-3722.
33. H. Y. Chen, S. Maiti and D. H. Son, *ACS Nano*, 2012, **6**, 583-591.
34. J. F. Suyver, S. F. Wuister, J. J. Kelly and A. Meijerink, *Phys. Chem. Chem. Phys.*, 2000, **2**, 5445-5448.
35. S. Mahamuni, A. D. Lad and S. Patole, *J. Phys. Chem. C*, 2008, **112**, 2271-2277.
36. J. Hu, L. S. Li, W. Yang, L. Manna, L. W. Wang and A. P. Alivisatos, *Science*, 2001, **292**, 2060-2063.
37. J. Wang, M. S. Gudixsen, X. Duan, Y. Cui and C. M. Lieber, *Science*, 2001, **293**, 1455-1457.
38. D. Rossi, J. H. Han, W. Jung, J. Cheon and D. H. Son, *ACS Nano*, 2015, **9**, 8037-8043.

Table of contents:



Manganese ions were incorporated into CsPbX₃ nanocrystals with their morphology and size preserved using a photo-induced post-synthesis doping method.